AIMS Mathematics, 11(11): 36723–36746.
DOI: 10.3934/math.20261420
Received: 01 August 2026
Revised: 05 October 2026
Accepted: 19 October 2026
Published: 06 November 2026

https://www.aimspress.com/journal/Math

Research article

Stability and Hopf bifurcation of a predator-prey model with hunting cooperation and group defense

Huisen Zhang*

Department of Basic Sciences, Lanzhou Institute of Technology, Lanzhou 730050, China

* **Correspondence:** Email: zhanghuisen0911@163.com.

Abstract: This work constructed a predator-prey model incorporating hunting cooperation and group defense, and explored its dynamical behavior. First, for the non-spatial model, the existence and local asymptotical stability of all feasible equilibria for the model were analyzed. Furthermore, the existence of Hopf bifurcation was investigated, and the occurrence direction of Hopf bifurcation as well as the stability and evolutionary characteristics of bifurcated periodic solutions were determined based on bifurcation theory. Second, a reaction-diffusion model was established by introducing spatial self-diffusion effects. The Turing instability of the positive equilibrium was emphatically studied, and the results verified that diffusion serves as a core inducement for Turing instability and spatial pattern formation. Meanwhile, the existence, direction, and stability of Hopf bifurcation in the diffusion system were analyzed, revealing the regulatory mechanism of spatial diffusion on system dynamical behavior. Finally, numerical simulations were carried out to validate the theoretical analyses and intuitively demonstrate the evolution processes of equilibria stability, bifurcation phenomena, and Turing instability.

Keywords: hunting cooperation; group defense; Hopf bifurcation; Turing instability
Mathematics Subject Classification: 34K13, 34K20, 35B32, 37G15

1. Introduction

Population dynamics is an important research field in biomathematics, aiming to explore the changes in the size of biological populations over time, and the predator-prey interaction plays a significant role in explaining the population dynamics of many species. In the early 20th century, Lotka and Volterra independently established the Lotka-Volterra model to describe the dynamics of the interaction between two species [1, 2]. Due to its universality and ecological relevance, predator-prey dynamics has since become a key research topic in theoretical ecology and mathematical ecology.

In natural ecosystems, prey populations commonly exhibit group defense behaviors when

perceiving predation risks. Group defense is a collective survival strategy in which individuals of the same species aggregate to form interdependent colonies to improve their survival chances. For prey with such defensive behavior, predators can only capture individuals located on the periphery of the aggregated group [3, 4]. This mechanism greatly reduces prey detectability, curbing predator population growth and even leading to local predator extinction [5–7]. This defensive strategy is widespread in nature, such as flocks of sheep and herds of cattle in grassland ecosystems and schools of sardines in marine environments [8, 9].

Nevertheless, classical functional responses are developed under the assumption of random interspecific encounters, where all prey face identical predation risk. This premise fails to characterize the non-uniform predation scenario induced by prey group defense. To address this limitation, Ajraldi and Braze proposed a novel functional response to incorporate group defense mechanisms [10, 11]. Specifically, Braze modified the classical Holling type-I functional response into a square-root form and established the corresponding predator-prey model

$$\begin{cases} \dfrac{\mathrm{d}N}{\mathrm{d}t} = rN\left(1 - \dfrac{N}{K}\right) - \lambda\sqrt{N}P, \\ \dfrac{\mathrm{d}P}{\mathrm{d}t} = e\lambda\sqrt{N}P - mP, \end{cases} \tag{1}$$

where N and P denote prey and predator population densities at time t, respectively, r is the per capita intrinsic growth rate of prey, K is the carrying capacity of the prey, λ stands for the attack rate of predators, e represents conversion efficiency, and m is the natural mortality rate of predators. Extensive dynamical investigations have been conducted on this model in the existing literature. Ajraldi et al. explored the stability of system equilibria [10]. Braze further analyzed the stability of interior equilibria, the existence of Hopf bifurcation, and trajectory distributions near the origin [11]. Furthermore, Manaf numerically verified that the model can generate transcritical, supercritical Hopf, and heteroclinic bifurcations, which significantly enrich the dynamical theories regarding prey group defense [12].

Hunting cooperation is a vital ecological phenomenon in predator-prey models [13–15]. Most biological populations exhibit cooperative behaviors for survival, reproduction, and population expansion, with hunting cooperation as a classic case. It refers to coordinated collective predation adopted by predators during prey capture [16–18]. Hunting cooperation brings substantial ecological benefits: Individual predators collectively search for and attack prey to supply sufficient resources to the whole population and greatly improve individual foraging efficiency. However, extreme cooperation leads to negative outcomes. A dense conspecific population under limited natural resources intensifies intraspecific food competition, which may drive population extinction. Excessively intensive hunting cooperation also causes over-predation, generating adverse ecological effects [19]. Accordingly, the investigation of hunting cooperation carries profound implications for endangered species conservation and sustainable ecosystem management.

To reveal how predator hunting cooperation affects species extinction risks, Duarte et al. constructed a tri-trophic food-chain model incorporating hunting cooperation. Their research revealed that predators face higher extinction risk as intensity of hunting cooperation [20]. Berec pioneered a mathematical model accounting for hunting cooperation, which employed ordinary differential equations to characterize predator-prey interactions with Holling type-II functional responses. His

analysis indicated that hunting cooperation exerts a destabilizing effect on predator-prey dynamics [21]. Subsequently, Alves and Hilker developed a series of predator-prey models integrating hunting cooperation and Holling-type functional responses. In their framework, predator attack rates increase monotonically with a predator density due to hunting cooperation [19]. The specific predator-prey model with Holling type-I functional response takes the following form:

$$\begin{cases} \dfrac{\mathrm{d}N}{\mathrm{d}t} = rN\left(1 - \dfrac{N}{K}\right) - (\lambda + aP)NP, \\ \dfrac{\mathrm{d}P}{\mathrm{d}t} = e(\lambda + aP)NP - mP, \end{cases} \tag{2}$$

where a represents the intensity coefficient of hunting cooperation, and the term aP quantifies the collective cooperative effect among predators. A series of rigorous theoretical analyses have been carried out on this model. Alves and Hilker numerically showed that the model admits complex dynamical behavior [19]. Zhang and Zhang further validated these results via qualitative bifurcation analysis and numerical simulations, and obtained the associated qualitative parameter conditions [22]. Wu and Zhao studied the impacts of spatial diffusion on model dynamics [23]. Song et al. analyzed system stability and Turing instability triggered by cross-diffusion [24]. With sophisticated analytical approaches, Li et al. derived the global dynamics of the model and uncovered how hunting cooperation intensity and the basic reproduction number regulate population evolution [25]. Apart from these works, numerous scholars have performed thorough analyses on the dynamical properties of this class of models [26, 27]. Further analytical results concerning such model dynamics are documented in [28, 29]. Additional relevant studies can be found in [30–32].

Inspired by [11] and [19], we naturally construct the following predator-prey model incorporating both prey group defense and predator hunting cooperation mechanisms,

$$\begin{cases} \dfrac{\mathrm{d}N}{\mathrm{d}t} = rN\left(1 - \dfrac{N}{K}\right) - (\lambda + aP)\sqrt{N}P, \\ \dfrac{\mathrm{d}P}{\mathrm{d}t} = e(\lambda + aP)\sqrt{N}P - mP. \end{cases} \tag{3}$$

These ecological interactions can be observed in real ecosystems, for instance, African wild dogs hunting wildebeest and impalas in savanna systems, and sailfish preying on schooling sardines in marine environments. In these systems, predators perform cooperative hunting to improve capture efficiency, while prey aggregate to form group defense, such that predators can only capture individuals on the periphery of prey aggregations rather than those inside the group. This biological setting is consistent with the assumptions of our predator-prey model.

To simplify the model structure, eliminate redundant parameter interference, reduce the number of free parameters, and facilitate subsequent dynamical theoretical analysis, we perform a dimensionless transformation on the model. The scaling aims to retain the core ecological mechanisms (prey group defense and predator hunting cooperation) while removing physically irrelevant dimensional constants, which makes the bifurcation thresholds and stability conditions easier to interpret.

We define the dimensionless state variables and time as

$$u = \frac{e^2\lambda^2}{m^2}N, \quad v = \frac{e\lambda^2}{m^2}P, \quad \tau = mt.$$

The dimensionless parameters are set as

$$\sigma = \frac{r}{m}, \quad \kappa = \frac{e^2\lambda^2 K}{m^2}, \quad \alpha = \frac{am^2}{e\lambda^3}.$$

For notational simplicity, we rename the dimensionless time τ back to t in the remainder of the paper, and then model (3) takes the form

$$\begin{cases} \dfrac{\mathrm{d}u}{\mathrm{d}t} = \sigma u\left(1 - \dfrac{u}{\kappa}\right) - (1 + \alpha v)\sqrt{u}v, \\ \dfrac{\mathrm{d}v}{\mathrm{d}t} = (1 + \alpha v)\sqrt{u}v - v. \end{cases} \tag{4}$$

This rescaling is a standard linear transformation of variables and time. It preserves all qualitative dynamical properties of the original system (3), including equilibrium existence, stability types, bifurcation sequences, and bifurcation directions. The bifurcation thresholds in the dimensionless model can be mapped back to the original dimensional parameters by inverse transformation, so the ecological interpretation of critical thresholds remains consistent.

The evolution of natural populations involves not only temporal dynamical variations but also spatial migration and diffusion behaviors. Populations spontaneously migrate from high-density areas to low-density regions to obtain survival resources and avoid predation risks, leading to spatially heterogeneous population distributions. Ordinary differential equations (ODEs) cannot capture such spatial population evolution, while reaction-diffusion models effectively couple temporal evolution and spatial diffusion. These models can accurately describe ecological phenomena, including population spatial distribution, spatial pattern formation, and species invasion [33, 34]. On this basis, we further introduce self-diffusion effects and establish the corresponding reaction-diffusion model associated with the above ODE model:

$$\begin{cases} u_t = d_1\Delta u + \sigma u\left(1 - \dfrac{u}{\kappa}\right) - (1 + \alpha v)\sqrt{u}v, & x \in \Omega,\ t > 0, \\ v_t = d_2\Delta v + (1 + \alpha v)\sqrt{u}v - v, & x \in \Omega,\ t > 0, \\ \partial_\nu u = \partial_\nu v = 0, & x \in \partial\Omega,\ t > 0, \\ u(x, 0) = u_0(x),\ v(x, 0) = v_0(x), & x \in \Omega, \end{cases} \tag{5}$$

where $\Omega \subset \mathbb{R}^N$ denotes a bounded domain with smooth boundary $\partial\Omega$, ν is the outward unit normal vector on $\partial\Omega$, and $\partial_\nu = \partial/\partial\nu$. The positive constants d_1 and d_2 represent the self-diffusion coefficients of u and v, respectively. Homogeneous Neumann boundary conditions indicate that model (5) is a closed ecological system, i.e., no population flux crosses the boundary $\partial\Omega$. The initial functions $u_0(x)$ and $v_0(x)$ are smooth, non-negative, and non-identically zero over Ω.

The paper is organized as follows. Section 2 is dedicated to the dynamics analysis of ODE model (4). We first investigate the existence and local stability of all nonnegative equilibria, then analyze the Hopf bifurcation emerging around the positive equilibrium, and finally, numerical simulations are further interpreted to illustrate the theoretical findings. Section 3 focuses on the spatial dynamics of reaction-diffusion model (5). We derive criteria for Turing instability at the positive

equilibrium, as well as the existence, bifurcation direction, and stability of periodic solutions induced by Hopf bifurcation, and a series of numerical simulations are carried out to validate all analytical results. Finally, Section 4 summarizes our main conclusions and provides concluding remarks.

2. Stability and bifurcations of non-spatial model (4)

2.1. Existence and stability of the equilibria

It is straightforward to verify that model (4) always admits two boundary equilibria $E_0 = (0, 0)$ and $E_1 = (\kappa, 0)$. In what follows, to yield the positive equilibria of model (4), we let

$$\begin{cases} f(u, v) := \sigma u\left(1 - \dfrac{u}{\kappa}\right) - (1 + \alpha v)\sqrt{u}\, v, \\ \\ g(u, v) := (1 + \alpha v)\sqrt{u}\, v - v. \end{cases}$$

Setting $f(u, v) = 0$ and $g(u, v) = 0$, by a direct calculation, we obtain

$$u = \frac{1}{(1 + \alpha v)^2},$$

and v satisfies

$$h(v) := \rho_5 v^5 + \rho_4 v^4 + \rho_3 v^3 + \rho_2 v^2 + \rho_1 v + \rho_0 = 0, \tag{6}$$

where $\rho_5 = \kappa\alpha^4$, $\rho_4 = 4\kappa\alpha^3$, $\rho_3 = 6\kappa\alpha^2$, $\rho_2 = \kappa\alpha(4 - \sigma\alpha)$, $\rho_1 = \kappa(1 - 2\sigma\alpha)$, $\rho_0 = \sigma(1 - \kappa)$. Now we explore the existence of positive roots of $h(v) = 0$ and compute the derivative

$$\frac{\mathrm{d}h(v)}{\mathrm{d}v} = \kappa(1 + \alpha v)(5\alpha^3 v^3 + 11\alpha^2 v^2 + 7\alpha v + 1 - 2\sigma\alpha).$$

Then we find that if $\alpha \le 1/(2\sigma)$, then $h'(v) > 0$, meaning that $h(v)$ is strictly increasing on $(0, +\infty)$. When $\kappa > 1$, it follows from $h(0) = \rho_0 < 0$ and $\lim\limits_{v\to+\infty} h(v) = +\infty$ that $h(v) = 0$ admits exactly one positive root. When $\kappa \le 1$, we have $h(0) = \rho_0 \ge 0$, combined with the monotonic increase of $h(v)$, we conclude that $h(v) = 0$ has no positive roots.

However, if $\alpha > 1/(2\sigma)$, there exists a threshold value $v_m > 0$ such that $h'(v) < 0$ for $v \in (0, v_m)$ and $h'(v) > 0$ for $v \in (v_m, +\infty)$. Accordingly, $h(v)$ decreases monotonically on $(0, v_m)$ and increases monotonically on $(v_m, +\infty)$, achieving its minimum value at v_m. Direct computation yields

$$v_m := \sqrt[3]{-\frac{q}{2} + \sqrt{\Upsilon}} + \sqrt[3]{-\frac{q}{2} - \sqrt{\Upsilon}} - \frac{11}{15\alpha},$$

where

$$p = -\frac{16}{75\alpha^2}, \quad q = -\frac{128 + 1350\sigma\alpha}{3375\alpha^3}, \quad \Upsilon = \left(\frac{q}{2}\right)^2 + \left(\frac{p}{3}\right)^3.$$

For $\kappa \ge 1$, the inequality $h(0) = \rho_0 < 0$ ensures that $h(v) = 0$ has a unique positive root. For $\kappa < 1$, the number of positive roots of $h(v) = 0$ is determined by the sign of $h(v_m)$. Define

$$\kappa_m := \frac{5\sigma\alpha}{(1 + \alpha v_m)^2 (1 + 3\sigma\alpha + \alpha v_m)}.$$

If $\kappa < \kappa_m$, then $h(v_m) < 0$, and hence $h(v) = 0$ has no positive roots; if $\kappa = \kappa_m$, then $h(v_m) = 0$, so $h(v) = 0$ has exactly one positive root $v^* = v_m$ satisfying $h'(v^*) = 0$; if $\kappa > \kappa_m$, then $h(v_m) > 0$, so $h(v) = 0$ has two distinct positive roots $v_1^* < v_m < v_2^*$ with $h'(v_1^*) > 0$ and $h'(v_2^*) < 0$.

The above analysis immediately leads to the theorem below.

Theorem 2.1. *For model (4), the following conclusions hold:*
(i) *If $\kappa > 1$, the model admits a unique positive equilibrium $E^* = (u^*, v^*)$;*
(ii) *If $\kappa = 1$ and $\alpha > 1/(2\sigma)$, the model possesses a unique positive equilibrium $E^* = (u^*, v^*)$;*
(iii) *If $\kappa \leq 1$ and $\alpha \leq 1/(2\sigma)$, the model has no positive equilibria;*
(iv) *Let $\kappa < 1$ and $\alpha > 1/(2\sigma)$:*
(iv-1) *if $\kappa < \kappa_m$, there exist no positive equilibria;*
(iv-2) *if $\kappa = \kappa_m$, the model has exactly one positive equilibrium $E^* = (u^*, v^*)$, where $v^* = v_m$;*
(iv-3) *if $\kappa > \kappa_m$, the model admits two distinct positive equilibria $E_1^* = (u_1^*, v_1^*)$ and $E_2^* = (u_2^*, v_2^*)$, satisfying $v_1^* < v_m < v_2^*$.*

We next employ the linearization method to investigate the local asymptotical stability of equilibria. Note that linearization at $E_0 = (0, 0)$ is not feasible for model (4); we only analyze the stability of E_1 and E^*. We first establish the following theorem.

Theorem 2.2. *For the semi-trivial equilibrium $E_1 = (\kappa, 0)$, if $\kappa < 1$, then E_1 is a locally asymptotically stable node; if $\kappa > 1$, then E_1 is a saddle point.*

Proof. The Jacobian matrix of model (4) evaluated at E_1 reads

$$J(E_1) = \begin{pmatrix} -\sigma & -\sqrt{\kappa} \\ 0 & \sqrt{\kappa} - 1 \end{pmatrix}.$$

The corresponding eigenvalues of $J(E_1)$ are $\lambda_1 = -\sigma < 0$ and $\lambda_2 = \sqrt{\kappa} - 1$. If $\kappa < 1$, we obtain $\lambda_2 < 0$, which implies that E_1 is a stable node. If $\kappa > 1$, $\lambda_2 > 0$, and hence E_1 is an unstable saddle point. □

We then analyze the local asymptotic stability of positive equilibria.

The Jacobian matrix of model (4) evaluated at the E^* takes the form

$$J(E^*) = \begin{pmatrix} f_{10} & f_{01} \\ g_{10} & g_{01} \end{pmatrix}, \tag{7}$$

where

$$\begin{aligned} f_{10} &= -\frac{\sigma}{\kappa(1+\alpha v^*)^2} + \frac{v^*(1+\alpha v^*)^2}{2}, \qquad f_{01} = -\frac{1+2\alpha v^*}{1+\alpha v^*} < 0, \\ g_{10} &= \frac{v^*(1+\alpha v^*)^2}{2} > 0, \qquad\qquad g_{01} = \frac{\alpha v^*}{1+\alpha v^*} > 0. \end{aligned} \tag{8}$$

The characteristic equation is given by

$$\lambda^2 - \mathrm{tr}[J(E^*)]\lambda + \det[J(E^*)] = 0, \tag{9}$$

with

$$\det[J(E^*)] = \frac{v^* h'(v^*)}{2\kappa^2(1+\alpha v^*)^4}, \qquad \mathrm{tr}[J(E^*)] = \frac{\varphi(\alpha)}{2\kappa(1+\alpha v^*)^2},$$

and

$$\varphi(\alpha) := \kappa(2+\sigma)(1+\alpha v^*)^2 - 2\kappa(1+\alpha v^*) - 3\sigma.$$

The local stability of the positive equilibrium E^* is determined by the signs of $\det[J(E^*)]$ and $\mathrm{tr}[J(E^*)]$.

We first consider the case where $\kappa > 1$. Under this parameter regime, model (4) admits a unique positive equilibrium E^*. Since $h'(v^*) > 0$, we immediately obtain $\det[J(E^*)] > 0$. Thus the stability of E^* is governed by $\mathrm{tr}[J(E^*)]$, i.e., the sign of $\varphi(\alpha)$. From $h(v^*) = 0$, we derive

$$\frac{\partial v^*}{\partial \alpha} = -\frac{2\kappa(1+\alpha v^*)v^*\big(2(1+\alpha v^*)^2 v^* - \sigma\big)}{h'(v^*)}.$$

A direct computation gives

$$\frac{\mathrm{d}\varphi(\alpha)}{\mathrm{d}\alpha} = \frac{2\kappa^2(1+\alpha v^*)^4 v^*\Big((1+\sigma)(1+\alpha v^*) + \alpha v^*\Big)}{h'(v^*)} > 0,$$

which demonstrates that $\varphi(\alpha)$ is strictly increasing on $(0, +\infty)$. Define

$$\alpha^* := \frac{\kappa\Theta(1+\Theta)^4}{\sigma\big(\kappa(1+\Theta)^2 - 1\big)},$$

where

$$\Theta := \frac{-\kappa(1+\sigma) + \sqrt{\kappa(\kappa + \sigma(3+\sigma))(2+\sigma)}}{\kappa(2+\sigma)}.$$

Note that $\varphi(0) = \sigma(\kappa - 3)$, if $\kappa \geq 3$, and then $\varphi(\alpha) > \varphi(0) \geq 0$, so E^* is unstable. If $\kappa < 3$, there exists a threshold value α^* such that if $0 < \alpha < \alpha^*$, then $\varphi(\alpha) < 0$, and hence E^* is stable; if $\alpha > \alpha^*$, then $\varphi(\alpha) > 0$, and hence E^* is unstable.

When $\kappa = 1$ and $\alpha > 1/(2\sigma)$, we have $h'(v^*) > 0$, which yields $\det[J(E^*)] > 0$. Moreover, $\varphi(0) = -2\sigma < 0$. Thus, if $\alpha < \alpha^*$, E^* is stable; if $\alpha > \alpha^*$, E^* is unstable.

When $\kappa < 1$, $\alpha > 1/(2\sigma)$ and $\kappa = \kappa_m$, and we have $h'(v^*) = 0$, leading to $\det[J(E^*)] = 0$. It follows that one eigenvalue of the characteristic equation is $\lambda_1 = 0$. Recalling $\varphi(0) < 0$, we deduce the following: If $\alpha < \alpha^*$, then $\mathrm{tr}[J(E^*)] < 0$, so $\lambda_2 < 0$, and E^* is an attracting saddle node; if $\alpha > \alpha^*$, then $\mathrm{tr}[J(E^*)] > 0$, so $\lambda_2 > 0$, and E^* is a repelling saddle node; and if $\alpha = \alpha^*$, then $\mathrm{tr}[J(E^*)] = 0$, so $\lambda_2 = 0$, meaning the characteristic equation admits a zero eigenvalue of algebraic multiplicity two, and E^* is a cusp.

When $\kappa < 1$, $\alpha > 1/(2\sigma)$ and $\kappa > \kappa_m$, and we have $h'(v_1^*) < 0$ and $h'(v_2^*) > 0$. This gives $\det[J(E_1^*)] < 0$ and $\det[J(E_2^*)] > 0$, so the characteristic equation has one positive real eigenvalue and one negative real eigenvalue, and E_1^* is always an unstable saddle point. For E_2^*, if $\alpha < \alpha^*$, E_2^* is stable; if $\alpha > \alpha^*$, E_2^* is unstable.

Based on the above analysis, we establish the following stability theorem for model (4).

Theorem 2.3.
(i) *If $\kappa > 1$, then E^* is locally asymptotically stable when $\kappa < 3$ and $0 < \alpha < \alpha^*$, while E^* is unstable if $\kappa \geq 3$ or $\kappa < 3$ and $\alpha > \alpha^*$.*

(ii) *If* $\kappa = 1$ *and* $\alpha > 1/(2\sigma)$*, then* E^* *is locally asymptotically stable for* $\alpha < \alpha^*$*, and unstable for* $\alpha > \alpha^*$.
(iii) *If* $\kappa < 1$, $\alpha > 1/(2\sigma)$ *and* $\kappa = \kappa_m$*, and then* E^* *is a cusp when* $\alpha = \alpha^*$*;* E^* *is a saddle node when* $\alpha \neq \alpha^*$*. Specifically,* E^* *is repelling for* $\alpha > \alpha^*$ *and attracting for* $\alpha < \alpha^*$.
(iv) *If* $\kappa < 1$, $\alpha > 1/(2\sigma)$ *and* $\kappa > \kappa_m$*, and then* E_1^* *is always a saddle point;* E_2^* *is locally asymptotically stable for* $\alpha < \alpha^*$ *and unstable for* $\alpha > \alpha^*$.

Theorem 2.1 establishes the existence of the positive equilibrium point of the model, while Theorem 2.3 summarizes the stability of this positive equilibrium point. To visually demonstrate the dynamic behavior of the model, all the results are summarized in Table 1.

Table 1. Existence and local stability of positive equilibria. E^*, E_1^*, and E_2^* denote positive equilibria. LAS = locally asymptotically stable.

Parameter conditions	Positive equilibria	Dynamical properties
$\kappa > 1$	Unique E^*	LAS if $\kappa < 3, \alpha < \alpha^*$; unstable if $\kappa \geq 3$ or $\kappa < 3, \alpha > \alpha^*$.
$\kappa = 1, \alpha > \dfrac{1}{2\sigma}$	Unique E^*	LAS for $\alpha < \alpha^*$; unstable for $\alpha > \alpha^*$.
$\kappa \leq 1, \alpha \leq \dfrac{1}{2\sigma}$	No positive equilibria	——
$\kappa < 1, \alpha > \dfrac{1}{2\sigma}, \kappa < \kappa_m$	No positive equilibria	——
$\kappa < 1, \alpha > \dfrac{1}{2\sigma}, \kappa = \kappa_m$	Unique equilibrium E^*	Cusp for $\alpha = \alpha^*$; saddle node for $\alpha \neq \alpha^*$.
$\kappa < 1, \alpha > \dfrac{1}{2\sigma}, \kappa > \kappa_m$	Two equilibria E_1^*, E_2^*	E_1^* is always a saddle point; E_2^* is LAS for $\alpha < \alpha^*$; unstable for $\alpha > \alpha^*$.

2.2. Hopf bifurcation analysis

In this subsection, we treat α as the bifurcation parameter and investigate the Hopf bifurcation of model (4) occurring at E^*.

Let $\lambda = \beta(\alpha) \pm \mathrm{i}\omega(\alpha)$ denote the root of Eq (9). If $1 < \kappa < 3$ is satisfied, evaluating at $\alpha = \alpha^*$ yields $\mathrm{tr}[J(E^*)] = 0$ and $\det[J(E^*)] > 0$. This implies Eq (9) admits a pair of pure imaginary roots

$$\lambda_{1,2} = \pm \mathrm{i}\sqrt{\det[J(E^*)]}.$$

At $\alpha = \alpha^*$, direct computation gives

$$\left.\frac{\mathrm{d}\,\mathrm{Re}\{\lambda\}}{\mathrm{d}\alpha}\right|_{\alpha=\alpha^*} = \left.\frac{\mathrm{d}\beta(\alpha)}{\mathrm{d}\alpha}\right|_{\alpha=\alpha^*} = \frac{\varphi'(\alpha^*)}{4\kappa(1+\alpha^* v^*)^2} > 0.$$

Consequently, by Poincaré-Andronov-Hopf bifurcation theorem [35], model (4) undergoes a Hopf bifurcation at E^* as $\alpha = \alpha^*$.

To reveal the detailed behavior near $\alpha = \alpha^*$, we further derive the corresponding normal form.

We translate the positive equilibrium $E^* = (u^*, v^*)$ to the origin via the coordinate translations $\bar{u} = u - u^*$ and $\bar{v} = v - v^*$. For notational simplicity, we drop the overbars and continue to write u and

v in place of $\bar{u}$ and $\bar{v}$. Then model (4) becomes

$$\begin{cases} \dfrac{\mathrm{d}u}{\mathrm{d}t} = f_{10}u + f_{01}v + f_{20}u^2 + f_{11}uv + f_{02}v^2 + f_{30}u^3 + f_{21}u^2v + f_{12}uv^2 + f_{03}v^3 + \cdots, \\ \dfrac{\mathrm{d}v}{\mathrm{d}t} = g_{10}u + g_{01}v + g_{20}u^2 + g_{11}uv + g_{02}v^2 + g_{30}u^3 + g_{21}u^2v + g_{12}uv^2 + g_{03}v^3 + \cdots, \end{cases} \tag{10}$$

where

$$\begin{aligned} f_{20} &= -\frac{\sigma}{\kappa} + \frac{1}{8}(1+\alpha v^*)^4 v^*, & g_{20} &= -\frac{1}{8}(1+\alpha v^*)^4 v^*, \\ f_{11} &= -g_{11} = -\frac{1}{2}(1+\alpha v^*)(1+2\alpha v^*), & f_{02} &= -g_{02} = -\frac{\alpha}{1+\alpha v^*}, \\ f_{30} &= -g_{30} = -\frac{1}{16}(1+\alpha v^*)^6 v^*, & f_{21} &= -g_{21} = \frac{1}{8}(1+\alpha v^*)^3(1+2\alpha v^*), \\ f_{12} &= -g_{12} = -\frac{1}{2}\alpha(1+\alpha v^*), & f_{03} &= -g_{03} = 0. \end{aligned}$$

The eigenvector corresponding to $\lambda = \beta(\alpha) \pm \mathrm{i}\omega(\alpha)$ is $\nu = (1, P - \mathrm{i}Q)^\top$, where

$$P = \frac{\beta(\alpha) - f_{10}}{f_{01}}, \qquad Q = -\frac{\omega(\alpha)}{f_{01}}.$$

We define

$$P^* = P\big|_{\alpha=\alpha^*}, \qquad Q^* = Q\big|_{\alpha=\alpha^*}, \qquad \omega^* = \omega(\alpha^*).$$

We introduce the transformation matrix

$$S = (\mathrm{Re}(\nu), -\mathrm{Im}(\nu)) = \begin{pmatrix} 1 & 0 \\ P & Q \end{pmatrix}.$$

Applying the transformation $(u, v)^\top = S(x, y)^\top$ to model (10), we get

$$\begin{cases} \dfrac{\mathrm{d}x}{\mathrm{d}t} = \beta(\alpha)x - \omega(\alpha)y + F(x, y, \alpha), \\ \dfrac{\mathrm{d}y}{\mathrm{d}t} = \omega(\alpha)x + \beta(\alpha)y + G(x, y, \alpha), \end{cases} \tag{11}$$

where

$$\begin{aligned} F(x, y, \alpha) = {} & (f_{20} + f_{11}P + f_{02}P^2)x^2 + (f_{11} + 2f_{02}P)Qxy + f_{03}Q^2y^2 \\ & + (f_{30} + f_{21}P + f_{12}P^2)x^3 + (f_{21} + 2f_{12}P)Qx^2y + f_{12}Q^2xy^2 + \cdots, \\ G(x, y, \alpha) = {} & -\frac{P}{Q}F(x, y, \alpha) + \frac{1}{Q}g_1(x, y, \alpha), \end{aligned}$$

with

$$\begin{aligned} g_1(x, y, \alpha) = {} & (g_{20} + g_{11}P + g_{02}P^2)x^2 + (g_{11} + 2g_{02}P)Qxy + g_{03}Q^2y^2 \\ & + (g_{30} + g_{21}P + g_{12}P^2)x^3 + (g_{21} + 2g_{12}P)Qx^2y + g_{12}Q^2xy^2 + \cdots. \end{aligned}$$

Rewrite (11) into polar coordinates,

$$\begin{cases} \dot{r} = \beta(\alpha)r + a(\alpha)r^3 + \cdots, \\ \dot{\theta} = \omega(\alpha) + c(\alpha)r^2 + \cdots. \end{cases} \tag{12}$$

Expanding (12) in a Taylor series around $\alpha = \alpha^*$ yields

$$\begin{cases} \dot{r} = \beta'(\alpha^*)(\alpha - \alpha^*)r + a(\alpha^*)r^3 + \cdots, \\ \dot{\theta} = \omega(\alpha^*) + \omega'(\alpha^*)(\alpha - \alpha_1) + c(\alpha^*)r^2 + \cdots. \end{cases} \tag{13}$$

To determine the stability of the bifurcating periodic solution, we evaluate the sign of coefficient $a(\alpha^*)$, defined as

$$\begin{aligned} a(\alpha^*) := & \frac{1}{16}(F_{xxx} + F_{xyy} + G_{xxy} + G_{yyy}) \\ & + \frac{1}{16\omega^*}[F_{xy}(F_{xx} + F_{yy}) - G_{xy}(G_{xx} + G_{yy}) - F_{xx}G_{xx} + F_{yy}G_{yy}], \end{aligned} \tag{14}$$

where all the partial derivatives are evaluated at the bifurcation point $(x, y, \alpha) = (0, 0, \alpha^*)$, and the relevant partial derivatives read

$$\begin{aligned} &F_{xxx}(\alpha^*) = 6(f_{30} + f_{21}P^* + f_{12}P^{*2}), && F_{xyy}(\alpha^*) = 2f_{12}Q^{*2}, \\ &G_{xxy}(\alpha^*) = -2(f_{21} + 2f_{12}P^*)(1 + P^*), && G_{yyy}(\alpha^*) = 0, \\ &F_{xx}(\alpha^*) = 2[(f_{11} + f_{02}P^*)P^* + f_{20}], && F_{xy}(\alpha^*) = (f_{11} + 2f_{02}P^*)Q^*, \\ &F_{yy}(\alpha^*) = 2f_{02}Q^{*2}, && G_{xx}(\alpha^*) = \frac{2\sigma}{\kappa} \cdot \frac{1}{Q^*} - F_{xx}(\alpha^*)\frac{1 + P^*}{Q^*}, \\ &G_{xy}(\alpha^*) = -F_{xy}(\alpha^*)\frac{1 + P^*}{Q^*}, && G_{yy}(\alpha^*) = -F_{yy}(\alpha^*)\frac{1 + P^*}{Q^*}. \end{aligned}$$

Define the first Liapunov coefficient

$$\mu_2 = -\frac{a(\alpha^*)}{\beta'(\alpha^*)}.$$

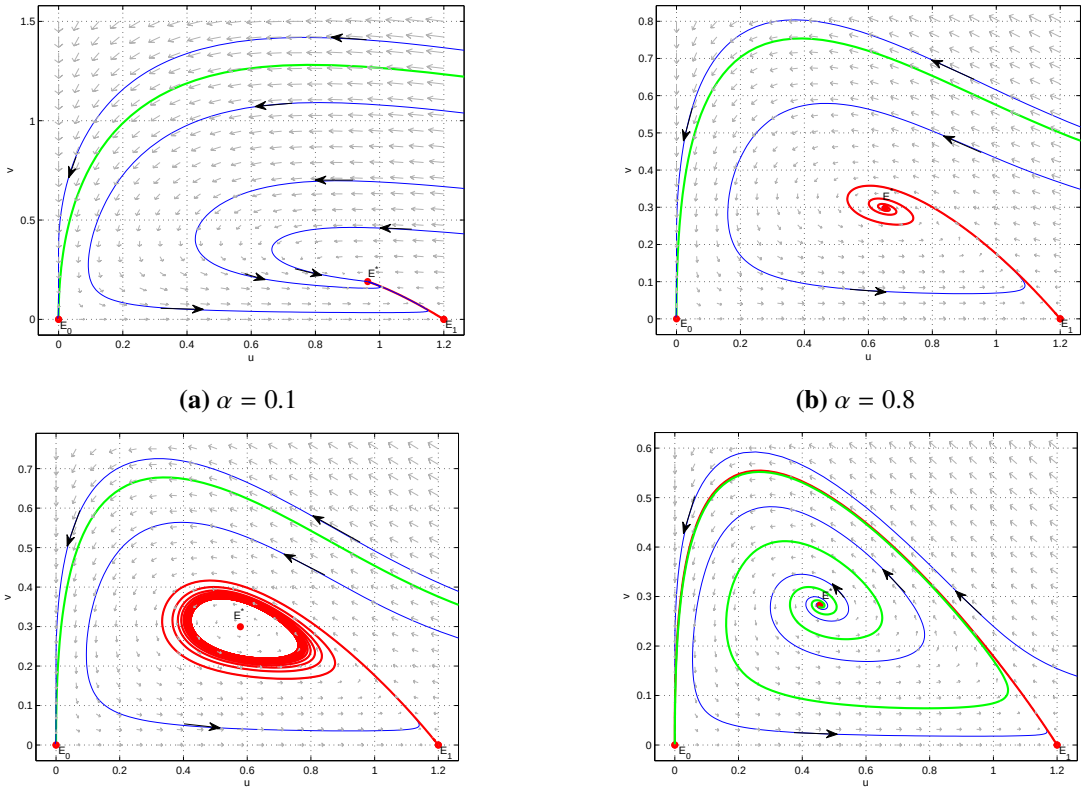
Recall that $\beta'(\alpha)|_{\alpha=\alpha^*} > 0$. We now state the following conclusion.

Theorem 2.4. *Assume $1 < \kappa < 3$. Then model (4) undergoes a Hopf bifurcation at E^* when $\alpha = \alpha^*$, where α^* satisfies relation (14). Moreover,*
(i) *if $a(\alpha^*) < 0$, the Hopf bifurcation is supercritical, and the bifurcating periodic solutions are orbitally asymptotically stable.*
(ii) *if $a(\alpha^*) > 0$, the Hopf bifurcation is subcritical, and the bifurcating periodic solutions are unstable.*

2.3. Numerical simulations

In this subsection, numerical simulations are carried out to verify the theoretical results obtained above.

Example 2.1. *Fix parameters $\sigma = 1$, $\kappa = 1.2$. Model (4) possesses three equilibria: two saddle points $E_0 = (0, 0)$ and $E_1 = (1.2, 0)$, together with a positive equilibrium $E^* = (u^*, v^*)$. There exists a separatrix in the phase plane that divides trajectories into two regions. Trajectories above this separatrix converge to the v-axis as $t \to +\infty$, implying that the prey species eventually go extinct. When $\alpha = 0.1$, $E^* = (0.9630, 0.1902)$ is a stable node (see Figure 1(a)). When $\alpha = 0.8$, $E^* = (0.6523, 0.2977)$ becomes a stable spiral sink (see Figure 1(b)). When $\alpha = 1.05$, $E^* = (0.5786, 0.2996)$ turns into an unstable spiral source, and the model admits a stable limit cycle (see Figure 1(c)). When $\alpha = 1.7$, the limit cycle disappears, and $E^* = (0.4561, 0.2828)$ is an unstable node source. The manifolds associated with E_0 intersect the u–axis and form a closed loop. All trajectories inside this closed loop originate near E^* and eventually approach E_0 (see Figure 1(d)). This phenomenon indicates that both prey and predator species will go extinct in the long run. The change in hunting cooperation rate α triggers Hopf bifurcation, altering the stability of positive equilibrium and governing the transition between stable coexistence, periodic coexistence, and global extinction of the two species.*



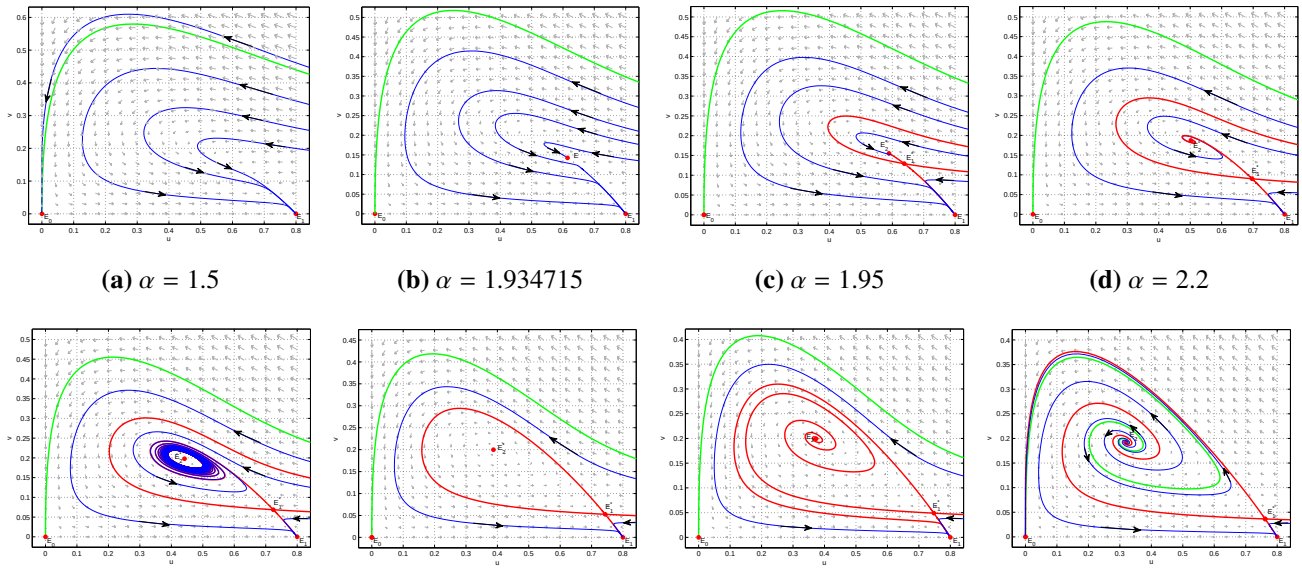
(a) $\alpha = 0.1$ **(b)** $\alpha = 0.8$

(c) $\alpha = 1.05$ **(d)** $\alpha = 1.7$

Figure 1. Phase portraits of model (4) with fixed $\sigma = 1$, $\kappa = 1.2$, where the model admits a unique positive equilibrium.

Example 2.2. *Fix parameters $\sigma = 1$, $\kappa = 0.8$. Model (4) always admits two boundary equilibria: a saddle point $E_0 = (0, 0)$ and a stable node $E_1 = (0.8, 0)$. For $\alpha = 1.5$, the model has no positive equilibrium (see Figure 2(a)), which means that the predator population cannot persist under weak cooperative hunting and eventually dies out. For $\alpha = 1.934715$, the model possesses a unique positive equilibrium $E^* = (0.6145, 0.1425)$, which is an attracting saddle node. The system undergoes a saddle*

node bifurcation at E^* (see Figure 2(b)). This bifurcation gives the critical cooperation threshold for the emergence of predator-prey coexistence. For $\alpha = 1.95$, there exist two positive equilibria: $E_1^* = (0.6379, 0.1293)$ is a saddle point and $E_2^* = (0.5894, 0.1552)$ is a node sink (see Figure 2(c)). For $\alpha = 2.2$, $E_2^* = (0.5020, 0.1870)$ turns into a spiral sink (see Figure 2(d)). For $\alpha = 2.55$, E_2^* becomes a spiral source, and model (4) experiences a Hopf bifurcation, which generates a limit cycle surrounding E_2^* (see Figure 2(e)). This Hopf bifurcation destabilizes the steady coexistence and induces sustained periodic fluctuations of predator and prey abundances. When $\alpha = 3.036$, the limit cycle disappears and the system undergoes a homoclinic bifurcation (see Figure 2(f)). For $\alpha = 3.2$, the homoclinic loop is broken, and the stable and unstable manifolds associated with E_2^* exchange their positions (see Figure 2(g)). For $\alpha = 4$, the manifolds of E_0 form a closed loop together with the u-axis, and all trajectories inside this closed loop eventually converge to E_1 (see Figure 2(h)). Biologically, overly intense hunting cooperation reduces predation pressure, leading to predator extinction while prey survives at its environmental carrying capacity.

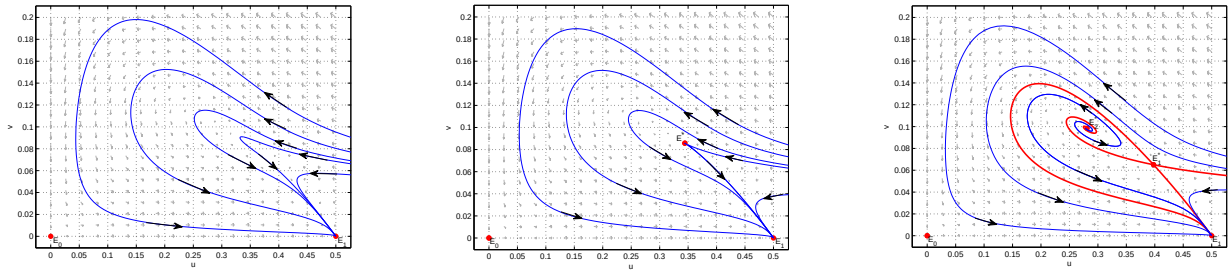


(a) $\alpha = 1.5$ **(b)** $\alpha = 1.934715$ **(c)** $\alpha = 1.95$ **(d)** $\alpha = 2.2$

(e) $\alpha = 2.55$ **(f)** $\alpha = 3.036$ **(g)** $\alpha = 3.2$ **(h)** $\alpha = 4$

Figure 2. Phase portraits of model (4) with fixed $\sigma = 1$, $\kappa = 0.8$, depicting the emergence and stability transitions of positive equilibria in the predator-prey model.

Example 2.3. *We fix $\sigma = 0.8$ and $\kappa = 0.5$, and gradually increase the intensity of predator hunting cooperation α to illustrate the cusp bifurcation. When the hunting cooperation rate is low ($\alpha = 8$), no positive equilibrium exists (see Figure 3(a)). As α increases to the critical value $\alpha = 8.21$, the model admits a unique positive equilibrium $E^* = (0.3442, 0.0858)$, which is a codimension-2 cusp singularity (see Figure 3(b)). This critical parameter threshold marks the minimum cooperation strength required for predator-prey coexistence. Under this degenerate state, tiny perturbations in species densities may trigger abrupt transitions between predator-prey coexistence and predator extinction. Further increasing α to $\alpha = 9$, the model yields two positive equilibria, where $E_1^* = (0.3978, 0.0651)$ is a saddle point and $E_2^* = (0.2811, 0.0985)$ is a spiral source (see Figure 3(c)). The red trajectory in the figure represents the separatrix, which divides the basins of attraction for different asymptotic states.*



(a) $\alpha = 2.2$ **(b)** $\alpha = 2.55$ **(c)** $\alpha = 3.036$

Figure 3. Phase portraits of model (4) with fixed $\sigma = 0.8$, $\kappa = 0.5$, illustrating cusp bifurcation induced by the variation of predator hunting cooperation intensity α.

3. Turing instability and bifurcation of diffusive model (5)

3.1. Stability and Turing instability

In this subsection, we investigate the stability of model (5) at positive equilibrium E^*. For the intuitive proof, we consider the one-dimensional spatial domain $\Omega = (0, \ell\pi)$. The linearization of model (5) at $E^* = (u^*, v^*)$ reads

$$\begin{pmatrix} u_t \\ v_t \end{pmatrix} = L\begin{pmatrix} u \\ v \end{pmatrix} := D\begin{pmatrix} \Delta u \\ \Delta v \end{pmatrix} + J(E^*)\begin{pmatrix} u \\ v \end{pmatrix}, \tag{15}$$

where $D = \mathrm{diag}(d_1, d_2)$ and $J(E^*)$ is given in (7). We seek general solutions to the linearied model (5) of the form

$$\begin{pmatrix} u \\ v \end{pmatrix} = \sum_{k=0}^{\infty} \begin{pmatrix} a_k \\ b_k \end{pmatrix} e^{\lambda t} \cos\frac{k}{\ell}x,$$

where $k \in \mathbb{N}_0 = \{0, 1, 2, \cdots\}$, λ denotes the growth rate of a small perturbation, and a_k and b_k are nonzero constants. Thereby, one has

$$\sum_{k=0}^{\infty} (J_k - \lambda I)\begin{pmatrix} a_k \\ b_k \end{pmatrix} \cos\frac{k}{\ell}x = 0,$$

where I stands for the identity matrix and

$$J_k := \begin{pmatrix} f_{10} - d_1\left(\frac{k}{\ell}\right)^2 & f_{01} \\ g_{10} & g_{01} - d_2\left(\frac{k}{\ell}\right)^2 \end{pmatrix}.$$

Consequently, we derive the characteristic equation

$$\Delta_k := \lambda^2 - T_k(\alpha)\lambda + D_k(\alpha) = 0, \qquad k \in \mathbb{N}_0, \tag{16}$$

where

$$T_k(\alpha) := \mathrm{tr}(J_k) = -(d_1 + d_2)\left(\frac{k}{\ell}\right)^2 + f_{10} + g_{01},$$

$$D_k(\alpha) := \det(J_k) = d_1 d_2\left(\frac{k}{\ell}\right)^4 - (g_{01}d_1 + f_{10}d_2)\left(\frac{k}{\ell}\right)^2 + f_{10}g_{01} - f_{01}g_{10}.$$

Theorem 3.1. *Assume* $1 < \kappa < 3$ *and* $0 < \alpha < \alpha^*$.
(i) *If*

$$0 < d_1 \le -\frac{f_{10}}{g_{01}}d_2,$$

then E^* *is locally asymptotically stable;*
(ii) *If*

$$-\frac{f_{10}}{g_{01}}d_2 < d_1 < \frac{2[f_{10}g_{01} - f_{01}g_{10}] + \sqrt{4(f_{10}g_{01} - f_{01}g_{10})^2 - f_{10}^2 g_{01}^2}}{g_{01}^2}d_2 := d_1^+,$$

then E^* *is locally asymptotically stable;*
(iii) *If* $d_1 > d_1^+$, *then* E^* *is locally asymptotically stable for wave number* $k < k_-$ *or* $k > k_+$. *However, Turing instability occurs in model (5) whenever* $k_- < k < k_+$, *where*

$$k_\pm^2 := \frac{g_{01}d_1 + f_{10}d_2 \pm \sqrt{(g_{01}d_1 + f_{10}d_2)^2 - 4d_1d_2(f_{10}g_{01} - f_{01}g_{10})}}{2d_1d_2}\ell^2 > 0. \tag{17}$$

Proof. Notice that $T_k(\alpha) \le T_0(\alpha) = f_{10} + g_{01} < 0$ for all $k \in \mathbb{N}_0$. Therefore, the stability of E^* is only determined by the sign of $D_k(\alpha)$.
(i) If

$$0 < d_1 \le -\frac{f_{10}}{g_{01}}d_2,$$

we can verify

$$D_k(\alpha) \ge d_1 d_2\left(\frac{k}{\ell}\right)^4 + D_0(\alpha) > 0.$$

This ensures that all eigenvalues of characteristic Eq (16) have negative real parts. Hence, E^* is locally asymptotically stable.
(ii) For convenience, set

$$z = \left(\frac{k}{\ell}\right)^2.$$

Then

$$D(z) = d_1d_2z^2 - (g_{01}d_1 + f_{10}d_2)z + f_{10}g_{01} - f_{01}g_{10},$$

which is a quadratic polynomial in z with axis of symmetry

$$z_{\min} = \frac{g_{01}d_1 + f_{10}d_2}{2d_1d_2}.$$

Under the condition

$$d_1 > -\frac{f_{10}}{g_{01}}d_2,$$

we have $z_{\min} > 0$, and $D(z)$ attains its minimum value at $z_{\min}$. The existence of positive roots for $D(z) = 0$ depends on the discriminant

$$\delta_z = (g_{01}d_1 + f_{10}d_2)^2 - 4d_1d_2(f_{10}g_{01} - f_{01}g_{10}).$$

Setting $\delta_z = 0$ and solving for d_1 yields

$$d_1^{\pm} = \frac{2[f_{10}g_{01} - f_{01}g_{10}] \pm \sqrt{4(f_{10}g_{01} - f_{01}g_{10})^2 - f_{10}^2 g_{01}^2}}{g_{01}^2} d_2.$$

If $d_1^- < d_1 < d_1^+$, then $\delta_z < 0$ yields

$$\min_{z>0} D(z) = D(z_{\min}) = \frac{4d_1d_2(f_{10}g_{01} - f_{01}g_{10}) - (g_{01}d_1 + f_{10}d_2)^2}{4d_1d_2} > 0.$$

Hence $D_k(\alpha) > 0$ holds for all $k \in \mathbb{N}_0$, so E^* is locally asymptatically stable. Also, it can be checked that

$$d_1^- < -\frac{f_{10}}{g_{01}} d_2.$$

(iii) If $d_1 > d_1^+$, some simple analysis shows that $D(z) = 0$ admits two distinct positive real roots

$$z_{\pm} = \frac{g_{01}d_1 + f_{10}d_2 \pm \sqrt{(g_{01}d_1 + f_{10}d_2)^2 - 4d_1d_2(f_{10}g_{01} - f_{01}g_{10})}}{2d_1d_2} > 0.$$

Accordingly, we can claim that $D(z) > 0$ for $0 < z < z_-$ or $z > z_+$, while $D(z) < 0$ for $z_- < z < z_+$. Recall $z = (k/\ell)^2$, and we can infer that $D_k(\alpha) > 0$ for all $k \in \mathbb{N}_0$, when the wave number $k < k_-$ or $k > k_+$ is satisfied. In this case, all roots of Eq (16) possess negative real parts, and thus E^* is locally asymptotically stable. Meanwhile, there exist some $k \in \mathbb{N}_0 \setminus \{0\}$ satisfying $k_- < k < k_+$ such that $\min_k D_k(\alpha) < 0$, which implies that Eq (16) has at least one eigenvalue with a positive real part, which renders E^* as unstable. As a result, Turing instability emerges in the diffusive model (5) at E^*. □

3.2. Hopf bifurcation analysis

In this subsection, we perform Hopf bifurcation analysis for model (5). According to Theorem 2.3, the positive equilibrium E^* of the corresponding ODE model (4) is asymptotically stable when $1 < \kappa < 3$ and $\alpha < \alpha^*$. Besides, we also know $\mathrm{tr}[J(E^*)] = 0$ if and only if $\alpha = \alpha^*$. Thus, spatially homogeneous periodic solutions bifurcate near $\alpha = \alpha^*$ provided the transversality condition holds. We take α as the Hopf bifurcation parameter. Assume that characteristic equation $\Delta_0 = 0$ has a pair of complex roots $\lambda(\alpha) = \beta(\alpha) \pm \mathrm{i}\omega(\alpha)$, where

$$\beta(\alpha) = \frac{1}{2}T_0(\alpha), \quad \omega(\alpha) = \frac{1}{2}\sqrt{4D_0(\alpha) - T_0(\alpha)}, \quad \beta(\alpha^*) = 0,$$

and

$$\beta'(\alpha^*) = \frac{\varphi'(\alpha^*)}{4\kappa(1 + \alpha^* v^*)^2} > 0.$$

This verifies the transversality condition. Furthermore, the real part of $\lambda(\alpha)$ becomes negative as α increases crossing α^*. At $\alpha = \alpha^*$, $\Delta_0 = 0$ has a pair of purely imaginary roots $\pm i\omega^*(\omega^* = \omega(\alpha^*))$. Using the normal form method and center mainfold theorem in [35], we further investigate the direction of the Hopf bifurcation.

Let L^* denote the conjugate operator of L defined in (15). We can obtain

$$L^*(\alpha)\begin{pmatrix} u \\ v \end{pmatrix} := D\begin{pmatrix} \Delta u \\ \Delta v \end{pmatrix} + J^*(\alpha)\begin{pmatrix} u \\ v \end{pmatrix}, \tag{18}$$

where $J^* = J^\top(E^*)$. Define

$$q := \begin{pmatrix} q_1 \\ q_2 \end{pmatrix} = \begin{pmatrix} 1 \\ -\frac{s_1}{s_2} + \frac{\omega^*}{s_2}\mathrm{i} \end{pmatrix}, \qquad q^* := \begin{pmatrix} q_1^* \\ q_2^* \end{pmatrix} = \frac{s_2}{2\pi\omega^*}\begin{pmatrix} \frac{\omega^*}{s_2} + \frac{s_1}{s_2}\mathrm{i} \\ \mathrm{i} \end{pmatrix},$$

which satisfy $\langle q^*, q\rangle = 1$, $\langle q^*, \bar{q}\rangle = 0$, and $L(\alpha^*)q = \mathrm{i}\omega^* q$. Here

$$s_1 = f_{10}(\alpha^*) = -\frac{\alpha^* v^*}{1+\alpha^* v^*}, \qquad s_2 = f_{01}(\alpha^*) = -\frac{1+2\alpha^* v^*}{1+\alpha^* v^*}, \qquad \omega^* = \omega(\alpha^*) = \sqrt{D_0(\alpha^*)}.$$

The inner product $\langle \xi, \eta\rangle = \int_0^{\ell\pi} \bar{\xi}^\top \eta\, dx$ is defined on $L^2[(0, \ell\pi)] \times L^2[(0, \ell\pi)]$.

Define

$$Q_{qq} := \begin{pmatrix} c_n \\ d_n \end{pmatrix}\cos^2\frac{n}{\ell}x, \qquad Q_{q\bar{q}} := \begin{pmatrix} e_n \\ f_n \end{pmatrix}\cos^2\frac{n}{\ell}x, \qquad C_{qq\bar{q}} := \begin{pmatrix} g_n \\ h_n \end{pmatrix}\cos^3\frac{n}{\ell}x.$$

If $n = 0$, we simplify to

$$Q_{qq} = \begin{pmatrix} c_0 \\ d_0 \end{pmatrix}, \qquad Q_{q\bar{q}} = \begin{pmatrix} e_0 \\ f_0 \end{pmatrix}, \qquad C_{qq\bar{q}} = \begin{pmatrix} g_0 \\ h_0 \end{pmatrix},$$

with

$$\begin{aligned}
c_0 &:= f_{uu}q_1^2 + 2f_{uv}q_1q_2 + f_{vv}q_2^2 = 2f_{20} + 2f_{11}q_2 + 2f_{02}q_2^2,\\
d_0 &:= g_{uu}q_1^2 + 2g_{uv}q_1q_2 + g_{vv}q_2^2 = 2g_{20} + 2g_{11}q_2 + 2g_{02}q_2^2 = 2(f_{20}+g_{20}) - c_0,\\
e_0 &:= f_{uu}|q_1|^2 + f_{uv}(q_1\bar{q}_2 + \bar{q}_1q_2) + f_{vv}|q_2|^2 = 2f_{20} + f_{11}(q_2+\bar{q}_2) + 2f_{02}|q_2|^2,\\
f_0 &:= g_{uu}|q_1|^2 + g_{uv}(q_1\bar{q}_2 + \bar{q}_1q_2) + g_{vv}|q_2|^2 = 2g_{20} + g_{11}(q_2+\bar{q}_2) + 2g_{02}|q_2|^2 = 2(f_{20}+g_{20}) - e_0,\\
g_0 &:= f_{uuu}|q_1|^2q_1 + f_{uuv}(2|q_1|^2q_2 + q_1^2\bar{q}_2) + f_{uvv}(2q_1|q_2|^2 + \bar{q}_1q_2^2) + f_{vvv}|q_2|^2q_2\\
&\quad = 6f_{30} + 2f_{21}(2q_2+\bar{q}_2) + 2f_{12}(2|q_2|^2 + q_2^2),\\
h_0 &:= g_{uuu}|q_1|^2q_1 + g_{uuv}(2|q_1|^2q_2 + q_1^2\bar{q}_2) + g_{uvv}(2q_1|q_2|^2 + \bar{q}_1q_2^2) + g_{vvv}|q_2|^2q_2\\
&\quad = 6g_{30} + 2g_{21}(2q_2+\bar{q}_2) + 2g_{12}(2|q_2|^2 + q_2^2) = -g_0,
\end{aligned}$$

where all partial derivatives are evaluated at the point $(u, v, \alpha) = (0, 0, \alpha^*)$.

Let

$$\mathfrak{g}_{20} = \langle q^*, Q_{qq} \rangle, \quad \mathfrak{g}_{11} = \langle q^*, Q_{q\bar{q}} \rangle, \quad \mathfrak{g}_{21} = \langle q^*, C_{qq\bar{q}} \rangle.$$

Then we obtain

$$\begin{aligned}
\mathfrak{g}_{20} &= \frac{s_2}{2\omega^*}\left[\left(\frac{\omega^*}{s_2} - \frac{s_1}{s_2}\mathrm{i}\right)c_0 - \mathrm{i}d_0\right] \\
&= f_{20} - f_{11} + \left(2s_1 - \frac{s_1^2 + \omega^{*2}}{s_2}\right)\frac{f_{02}}{s_2} \\
&\quad - \frac{\mathrm{i}}{\omega^*}\left[s_1 f_{20} + s_2 g_{20} + \left(\omega^{*2} - s_1^2 + \frac{s_1(s_1^2 + \omega^{*2})}{s_2}\right)f_{02}\right], \\
\mathfrak{g}_{11} &= \frac{s_2}{2\omega^*}\left[\left(\frac{\omega^*}{s_2} - \frac{s_1}{s_2}\mathrm{i}\right)e_0 - \mathrm{i}f_0\right] \\
&= f_{20} - \frac{s_1}{s_2}f_{11} + \frac{s_1^2 + \omega^{*2}}{s_2^2}f_{02} \\
&\quad - \frac{\mathrm{i}}{\omega^*}\left(s_1 f_{20} + s_2 g_{20} - \frac{s_1 - s_2}{s_2}s_1 f_{11} + \frac{(s_1 - s_2)(s_1^2 + \omega^{*2})}{s_2^2}f_{02}\right), \\
\mathrm{Re}\{\mathfrak{g}_{21}\} &= \mathrm{Re}\left\{\frac{s_2}{2\omega^*}\left[\left(\frac{\omega^*}{s_2} - \frac{s_1}{s_2}\mathrm{i}\right)g_0 - \mathrm{i}h_0\right]\right\} \\
&= 3f_{30} - \frac{2s_1 + s_2}{s_2}f_{21} + \frac{2s_1 s_2 + s_1^2 + \omega^{*2}}{s_2^2}f_{12}.
\end{aligned}$$

From [35], the direction and stability of the Hopf bifurcation are determined by the signs of μ_2 and ς, respectively, where

$$\mu_2 = \frac{\mathrm{Re}(c_1(\alpha^*))}{\beta'(\alpha^*)}, \qquad \varsigma = 2\mathrm{Re}(c_1(\alpha^*)),$$

and

$$\begin{aligned}
\mathrm{Re}(c_1(\alpha^*)) &:= \mathrm{Re}\left\{\frac{\mathrm{i}}{2\omega^*}\left(\mathfrak{g}_{20}\mathfrak{g}_{11} - 2|\mathfrak{g}_{11}|^2 - \frac{1}{3}|\mathfrak{g}_{02}|^2\right) + \frac{1}{2}\mathfrak{g}_{21}\right\} \\
&= -\frac{1}{2\omega^*}[\mathrm{Re}(\mathfrak{g}_{20})\,\mathrm{Im}(\mathfrak{g}_{11}) + \mathrm{Im}(\mathfrak{g}_{20})\,\mathrm{Re}(\mathfrak{g}_{11})] + \frac{1}{2}\,\mathrm{Re}(\mathfrak{g}_{21}).
\end{aligned} \tag{19}$$

Combined with the transversality condition and the above formula, we have the following results on the direction and stability of the Hopf bifurcation.

Theorem 3.2. *Assume $1 < \kappa < 3$. Then model (5) undergoes a Hopf bifurcation at $\alpha = \alpha^*$.*
(i) *If $\mathrm{Re}(c_1(\alpha^*)) < 0$, the Hopf bifurcation is supercritical, and the bifurcating periodic solutions are asymptotically stable on the center manifold;*
(ii) *If $\mathrm{Re}(c_1(\alpha^*)) > 0$, the Hopf bifurcation is subcritical, and the bifurcating periodic solutions are unstable.*

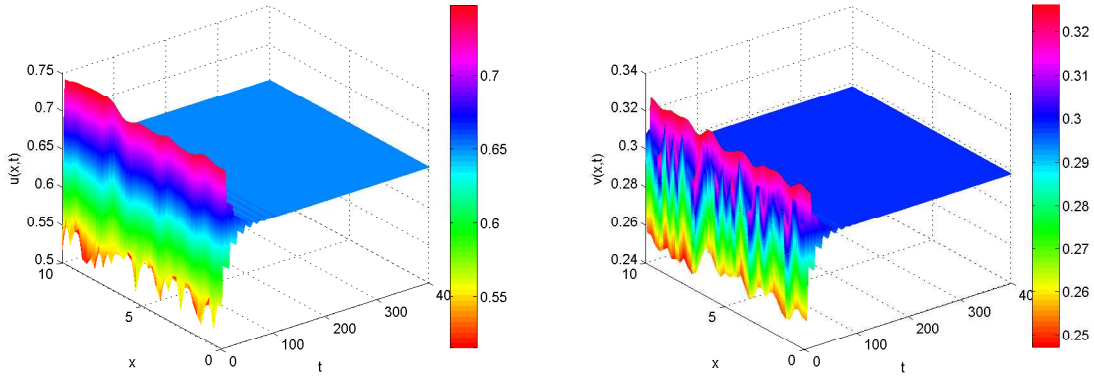
3.3. Numerical simulations

In this subsection, we carry out numerical examples to verify the theoretical analysis.

Example 3.1. *Let the spatial domain* $\Omega = (0, 10)$ *and fix the parameters*

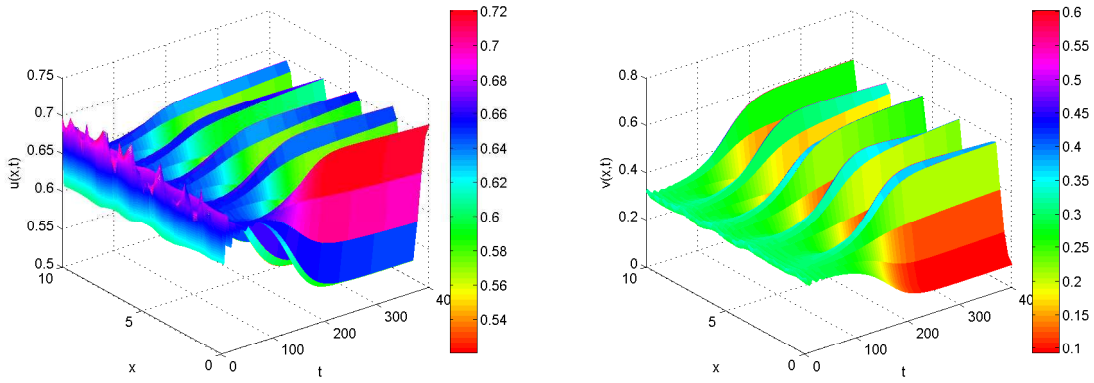
$$\sigma = 1,\ \kappa = 1.2,\ \alpha = 0.8,\ d_2 = 0.01. \tag{20}$$

Under such parameter settings, model (5) admits a unique positive equilibrium $E^* = (0.6523, 0.2977)$*, which is locally asymptotically stable for the corresponding ordinary differential equation model. For prey diffusion coefficient* $d_1 = 0.1$*,* E^* *remains locally asymptotically stable within the reaction-diffusion model (see Figure 4). Increasing the prey diffusion coefficient to* $d_1 = 0.4$*,* E^* *loses stability and Turing instability emerges in the model (see Figure 5). This observation reveals that the prey diffusion rate serves as a crucial factor modulating spatial population patterns. Weak prey diffusion cannot break the uniform coexistence steady state. Once prey diffusion exceeds the critical value, the coupling between spatial diffusion and interspecific predation drives uniformly distributed populations to spontaneously segregate, leading to heterogeneous spatial distributions. Biologically, this Turing pattern formation implies that prey mobility can induce spatial aggregation of species, even when the well-mixed population tends to stabilize at a constant coexistence level.*



(a) **(b)**

Figure 4. Numerical simulations of the stable equilibrium of model (5) with parameters in (20) and $d_1 = 0.1$.



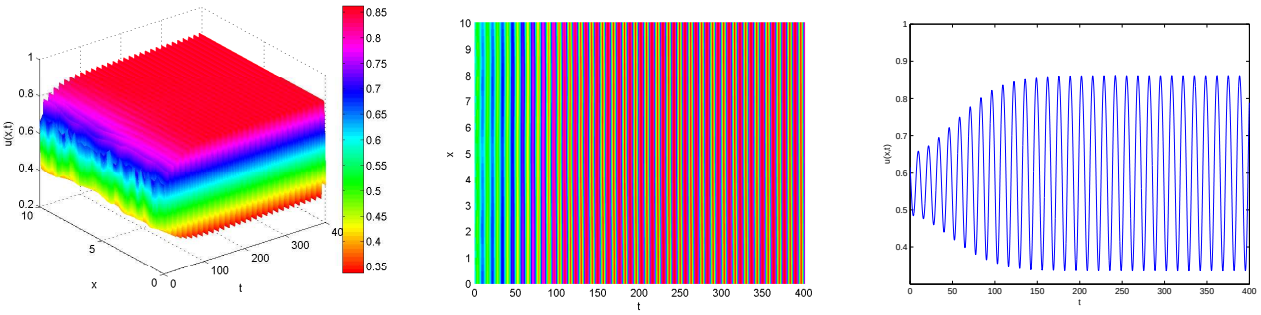
(a) **(b)**

Figure 5. Numerical simulations of the Turing instability of the equilibrium of model (5) with parameters in (20) and $d_1 = 0.4$.

Example 3.2. *We now explore how the predator hunting cooperation coefficient α affects Hopf bifurcating periodic solutions. Since the spatial distributions of the predator and prey exhibit similar characteristics, we only present the spatial distribution for the prey. Fix the parameters*

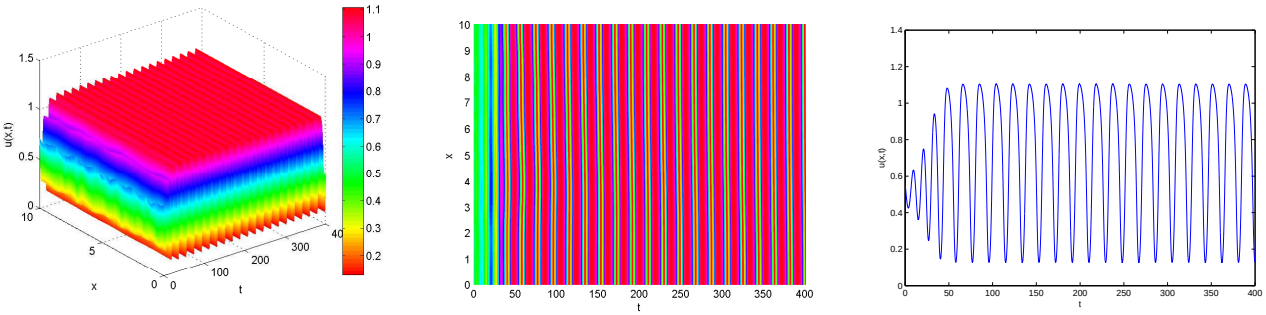
$$\sigma = 1, \quad \kappa = 1.2, \quad d_1 = 0.01, \quad d_2 = 0.01, \tag{21}$$

and choose $\alpha = 1.1, 1.35, 1.55$, respectively. The numerical outcomes for these three values of α are shown in Figures 6–8.



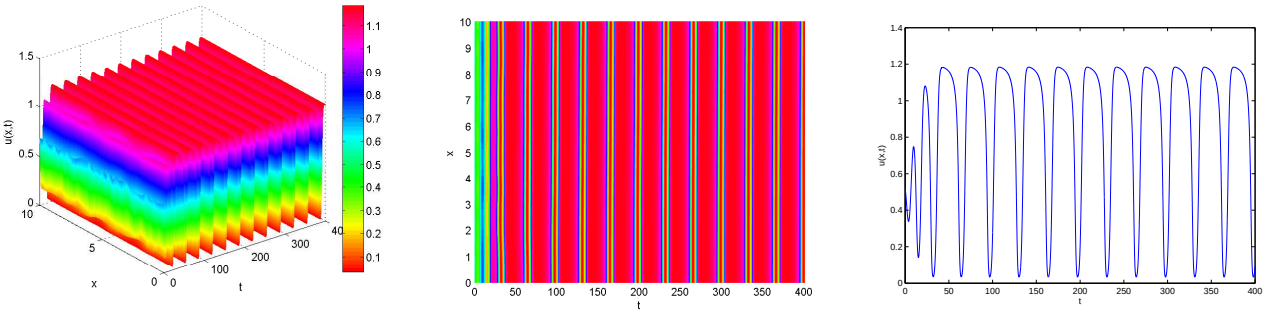
(a) **(b)** **(c)**

Figure 6. When $\alpha = 1.1$, the spatially homogeneous periodic solution of the prey is shown.



(a) **(b)** **(c)**

Figure 7. When $\alpha = 1.35$, the spatially homogeneous periodic solution of the prey is shown.



(a) **(b)** **(c)**

Figure 8. When $\alpha = 1.55$, the spatially homogeneous periodic solution of the prey is shown.

For these parameters, the model admits a unique unstable positive equilibrium, and Hopf bifurcating periodic solutions emerge around this equilibrium. Numerical results reveal that increasing α continuously lengthens the period of periodic solutions, while these periodic solutions remain stable throughout. This indicates that stronger hunting cooperation prolongs the time interval of predator-prey population cycles and moderates the periodic fluctuations between the two populations.

4. Conclusions and discussion

This paper investigates the dynamical behaviors of a predator-prey model incorporating hunting cooperation among predators and group defense of prey, and reveals how these two biological behaviors modulate population coexistence and system stability. The main conclusions are summarized as follows.

For the non-spatial model, we investigate equilibrium stability and bifurcation dynamics. First, we derive the threshold conditions for the existence of equilibria, and establish criteria for the local asymptotic stability of the positive equilibrium via linearization analysis. Second, using the Poincaré-Andronov-Hopf bifurcation theorem, the center manifold theorem, and normal form theory, we rigorously derive the existence conditions for Hopf bifurcation and determine the bifurcation direction and orbital stability of bifurcating periodic solutions. Finally, numerical simulations are carried out

to verify the validity of the theoretical results. Dynamical analysis indicates that hunting cooperation exhibits dual ecological effects. On one hand, it facilitates the coexistence of predators and prey, and improves the survival ability of predators. On the other hand, this behavior mechanism tends to destabilize the ecological system and can lead to abrupt regime shifts of the ecosystem. Meanwhile, group defense enables prey to resist predation pressure effectively and markedly elevates prey population density. Importantly, both biological behaviors possess ecological thresholds. Moderate hunting cooperation and group defense contribute to maintaining ecological balance. In contrast, excessive hunting cooperation intensifies interspecific predation, while excessively strong group defense breaks interspecific balance; both scenarios may result in species extinction and the collapse of local ecosystems.

For the reaction-diffusion predator-prey model, we explore diffusion-driven spatial dynamics. Theoretical analysis demonstrates that self-diffusion can alter the stability of the positive equilibrium and induce classical Turing instability, which gives rise to abundant spatial patterns. This provides a theoretical explanation for the formation of heterogeneous population distributions observed in natural ecosystems. Furthermore, bifurcation theory is adopted to analyze Hopf bifurcation within the diffusive model. The existence conditions, bifurcation direction, and stability of periodic solutions associated with spatially homogeneous Hopf bifurcation are clarified. The results uncover the inherent laws governing population oscillations and spatiotemporal evolution under the coupling of spatial diffusion and interspecific interactions. This study provides theoretical support for understanding periodic population fluctuations and spatial distribution patterns in nature.

Compared with the single mechanism models (1) and (2), the coupled predator-prey model (3) reveals some new dynamical behaviors resulting from the interaction of hunting cooperation and prey group defense. Hunting cooperation introduces new bifurcation scenarios that cannot be observed in the pure group defense model, while prey group defense makes the dynamical properties near the original equilibrium more complex. When only one biological mechanism is considered, this combined effect does not exist. The study shows that the coexistence of these two ecological behaviors can jointly reshape the threshold conditions for the existence of equilibrium, Hopf bifurcation, and Turing instability. These theoretical findings emphasize the importance of simultaneously incorporating multiple interspecies interactions when modeling natural ecosystems.

Nevertheless, the current model is formulated within the integer-order differential equation framework, which cannot capture memory effects and hereditary properties widely existing in real ecological communities. Additionally, deterministic equations ignore the random environmental noise and random fluctuations that are ubiquitous in natural ecosystems. In future investigations, we will extend the proposed predator-prey system to fractal-fractional frameworks with generalized fractional derivatives such as Atangana-Baleanu and Caputo-Fabrizio operators [36, 37]. Additionally, we will introduce random terms into the model to account for environmental randomness [38]. Based on the advanced theories and numerical methods of fractional and stochastic dynamical systems, the existence, stability, and bifurcation dynamics of the extended model will be further explored.

Use of Generative-AI tools declaration

The author declares she has not used Artificial Intelligence (AI) tools in the creation of this article.

Acknowledgments

This work is supported by Youth Science and Technology Innovation Project of Lanzhou Institute of Technology (No. 2025KJ-28).

Conflict of interest

The author declares no conflict of interest regarding the publication of this manuscript.

References

1. A. J. Lotka, Undamped oscillations derived from the law of mass action, *J. Am. Chem. Soc.*, **42** (1920), 1595–1599. https://doi.org/10.1021/ja01453a010
2. V. Volterra, Fluctuation in the abundance of a species considered mathematically, *Nature*, **118** (1926), 558–560. https://doi.org/10.1038/118558a0
3. R. Levins, Some demographic and genetic consequences of environmental heterogeneity for biological control, *Bull. Entomol. Soc. Am.*, **15** (1969), 237–240. https://doi.org/10.1093/besa/15.3.237
4. S. Wright, Breeding structure of populations in relation to speciation, *Am. Nat.*, **74** (1940), 232–248. https://doi.org/10.1086/280891
5. H. Freedman, G. Wolkowicz, Predator-prey systems with group defence: the paradox of enrichment revisited, *Bull. Math. Biol.*, **48** (1986), 493–508. https://doi.org/10.1007/BF02462320
6. H. Freedman, S. G. Ruan, Hopf bifurcation in three-species food chain models with group defense, *Math. Biosci.*, **111** (1992), 73–87. https://doi.org/10.1016/0025-5564(92)90079-C
7. M. Das, G. P. Samanta, A prey-predator fractional order model with fear effect and group defense, *Int. J. Dyn. Control*, **9** (2021), 334–349. https://doi.org/10.1007/s40435-020-00626-x
8. P. Brehmer, F. Gerlotto, C. Laurent, P. Cotel, A. Alina, B. Samb, Schooling behaviour of small pelagic fish: phenotypic expression of independent stimuli, *Mar. Ecol. Prog. Ser.*, **334** (2007), 263–272. https://doi.org/10.3354/meps334263
9. J. Zwolinski, D. Demer, A cold oceanographic regime with high exploitation rates in the Northeast Pacific forecasts a collapse of the sardine stock, *Proc. Natl. Acad. Sci. U. S. A.*, **109** (2012), 4175–4180. https://doi.org/10.1073/pnas.1113806109
10. V. Ajraldi, M. Pittavino, E. Venturino, Modelling herd behavior in population systems, *Nonlinear Anal. Real World Appl.*, **12** (2011), 2319–2338. https://doi.org/10.1016/j.nonrwa.2011.02.002
11. P. A. Braza, Predator-prey dynamics with square root functional responses, *Nonlinear Anal. Real World Appl.*, **13** (2012), 1837–1843. https://doi.org/10.1016/j.nonrwa.2011.12.014
12. Z. A. Manaf, H. M. Mohd, Bifurcation analysis of the prey-predator models incorporating herd behaviours, *IOP Conf. Ser. Earth Environ. Sci.*, **380** (2019), 012009. https://doi.org/10.1088/1755-1315/380/1/012009
13. D. P. Hector, Cooperative hunting and its relationship to foraging success and prey size in an avian predator, *Ethology*, **73** (1986), 247–257. https://doi.org/10.1111/j.1439-0310.1986.tb00915.x

14. D. Scheel, C. Packer, Group hunting behaviour of lions: a search for cooperation, *Anim. Behav.*, **41** (1991), 697–709. https://doi.org/10.1016/S0003-3472(05)80907-8

15. C. Boesch, Cooperative hunting in wild chimpanzees, *Anim. Behav.*, **48** (1994), 653–667. https://doi.org/10.1006/anbe.1994.1285

16. S. Creel, N. M. Creel, Communal hunting and pack size in African wild dogs, Lycaon pictus, *Anim. Behav.*, **50** (1995), 1325–1339. https://doi.org/10.1016/0003-3472(95)80048-4

17. P. A. Schmidt, L. D. Mech, Wolf pack size and food acquisition, *Am. Nat.*, **150** (1997), 513–517. https://doi.org/10.1086/286079

18. R. Bshary, A. Hohner, K. A. T. Djoudi, H. Fricke, Interspecific communicative and coordinated hunting between groupers and giant moray eels in the Red Sea, *PLoS Biol.*, **4** (2006), e431. https://doi.org/10.1371/journal.pbio.0040431

19. M. T. Alves, F. M. Hilker, Hunting cooperation and Allee effects in predators, *J. Theor. Biol.*, **419** (2017), 13–22. https://doi.org/10.1016/j.jtbi.2017.02.002

20. J. Duarte, C. Januario, N. Martins, J. Sardanyes, Chaos and crises in a model for cooperative hunting: a symbolic dynamics approach, *Chaos*, **19** (2009), 043102. https://doi.org/10.1063/1.3243924

21. L. Berec, Impacts of foraging facilitation among predators on predator-prey dynamics, *Bull. Math. Biol.*, **72** (2010), 94–121. https://doi.org/10.1007/s11538-009-9439-1

22. J. Zhang, W. N. Zhang, Dynamics of a predator-prey model with hunting cooperation and Allee effects in predators, *Int. J. Bifurcation Chaos*, **30** (2020), 2050199. https://doi.org/10.1142/S0218127420501990

23. D. Y. Wu, M. Zhao, Qualitative analysis for a diffusive predator-prey model with hunting cooperative, *Physica A*, **515** (2019), 299–309. https://doi.org/10.1016/j.physa.2018.09.176

24. D. X. Song, C. Li, Y. L. Song, Stability and cross-diffusion-driven instability in a diffusive predator-prey system with hunting cooperation functional response, *Nonlinear Anal. Real World Appl.*, **54** (2020), 103106. https://doi.org/10.1016/j.nonrwa.2020.103106

25. J. Q. Li, Y. M. Chen, N. N. Xue, P. J. Zhang, Z. W. Long, Y. Q. He, Impacts of hunting cooperation among predators on predator-prey dynamics, *J. Theor. Biol.*, **627** (2026), 112460. https://doi.org/10.1016/j.jtbi.2026.112460

26. S. Pal, N. Pal, S. Samanta, J. Chattopadhyay, Effect of hunting cooperation and fear in a predator-prey model, *Ecol. Complex.*, **39** (2019), 100770. https://doi.org/10.1016/j.ecocom.2019.100770

27. T. Singh, R. Dubey, V. N. Mishra, Spatial dynamics of predator-prey system with hunting cooperation in predators and Type I functional response, *AIMS Math.*, **5** (2019), 673–684. https://doi.org/10.3934/math.2020045

28. F. Capone, M. F. Carfora, R. De Luca, I. Torcicollo, Turing patterns in a reaction-diffusion system modeling hunting cooperation, *Math. Comput. Simul.*, **165** (2019), 172–180. https://doi.org/10.1016/j.matcom.2019.03.010

29. X. C. Hu, S. R. J. Jang, Stochasticity and cooperative hunting in predator-prey interactions, *J. Biol. Syst.*, **29** (2021), 525–541. https://doi.org/10.1142/S0218339021400040

30. N. Mukherjee, M. Banerjee, Hunting cooperation among slowly diffusing specialist predators can induce stationary Turing patterns, *Physica A*, **599** (2022), 127417. https://doi.org/10.1016/j.physa.2022.127417

31. J. Roy, S. Dey, B. W. Kooi, M. Banerjee, Prey group defense and hunting cooperation among generalist-predators induce complex dynamics: a mathematical study, *J. Math. Biol.*, **89** (2024), 22. https://doi.org/10.1007/s00285-024-02121-9

32. A. K. Umrao, P. K. Srivastava, Bifurcation analysis of a predator-prey model with Allee effect and fear effect in prey and hunting cooperation in predator, *Differ. Equ. Dyn. Syst.*, **33** (2025), 1123–1149. https://doi.org/10.1007/s12591-023-00663-w

33. R. A. Fisher, The waves of advance of advantageous genes, *Ann. Hum. Genet.*, **7** (1937), 355–369. https://doi.org/10.1111/j.1469-1809.1937.tb02153.x

34. B. Dubey, B. Das, J. Hussain, A predator-prey interaction model with self and cross-diffusion, *Ecol. Model.*, **141** (2011), 67–76. https://doi.org/10.1016/S0304-3800(01)00255-1

35. B. D. Hassard, N. D. Kazarinoff, Y. H. Wan, Theory and applications of Hopf bifurcation, In: *London mathematical society lecture note series*, Cambridge: Cambridge University Press, 1981. https://doi.org/10.1090/conm/445

36. W. Alsadi, Z. C. Wei, I. Moroz, A. Alkhazzan, Existence and stability of solution in Banach space for an impulsive system involving Atangana-Baleanu and Caputo-Fabrizio derivatives, *Fractals*, **31** (2023), 2340085. https://doi.org/10.1142/S0218348X23400856

37. W. Alsadi, Z. C. Wei, T. Q. S. Abdullah, A. Abdullah, J. F. Gomez-Aguilar, Dynamical and numerical analysis of the hepatitis B virus treatment model through fractal-fractional derivative, *Math. Methods Appl. Sci.*, **48** (2024), 639–657. https://doi.org/10.1002/mma.10348

38. Y. H. Lv, H. Wang, J. Ding, Q. X. Zhu, Dynamic analysis of a stochastic three species predator-prey model with intraguild predation and predator-switching, *Commun. Nonlinear Sci. Numer. Simul.*, **157** (2026), 109748. https://doi.org/10.1016/j.cnsns.2026.109748



AIMS Press

© 2026 the Author(s), licensee AIMS Press. This is an open access article distributed under the terms of the Creative Commons Attribution License (https://creativecommons.org/licenses/by/4.0)